Published on 29 July 2019. Downloaded by Korea Advanced Institute of Science & Technology / KAIST on 9/26/2019 4:29:01 AM.

Nanoscale

ROYAL SOCIETY OF CHEMISTRY

PAPER

View Article Online
View Journal | View Issue

Cite this: *Nanoscale*, 2019, **11**, 15374

Scratch to sensitize: scratch-induced sensitivity enhancement in semiconductor thin-film sensors†

Geonhee Lee,[a,b] Min Choi,[c,d] Soo Sang Chae,‡[a] Du Won Jeong,[a] Won Jin Choi,[a,e] Seulgi Ji,[a] Yun Ho Kim,[a] Ji Woon Choi,[f] Tae Il Lee,[g] Incheol Cho,[h] Inkyu Park,[h] Sun Sook Lee,[a] Sungsu Park,[i] Noejung Park,[j] Hyunju Chang[c] and Jeong-O. Lee *[a]

Received 10th May 2019,
Accepted 28th July 2019

DOI: 10.1039/c9nr03984h

rsc.li/nanoscale

Semiconductor gas sensors are advantageous in miniaturization and can be used in a wide range of applications, yet consume large power due to high operating temperature. Here we demonstrated the ability of nanoscale scratches produced with mechanical abrasion to enhance the chemical sensitivity of thin-film-type semiconductor sensors. Well-aligned arrays of scratches parallel to the electrical current direction between the source and drain electrodes were made, using typical polishing machines with diamond suspensions, on semiconductor thin films produced with various deposition methods such as atomic layer deposition (ALD), sputtering, and the sol–gel technique. Processing with sharp diamond microparticles left nano-grooves on the surface, together with changes in chemical composition. For all of the tested metal oxide thin films, the introduction of scratches yielded increased quantities of oxygen vacancies and metallic components. Scratched ZnO devices exhibited superior performance even at room temperature, as predicted by a computational simulation that showed increased binding energy of gas molecules on defects. The scratch technique shown in the present study may be used to produce dense arrays of nanometer-scale, chemically functionalized line patterns on substrates larger than a few tens of centimeters with minimum cost, which in turn may be used in a variety of applications including massive arrays of sensors displaying high sensitivity.

1. Introduction

Semiconductor devices are widely used as sensors of a variety of physical and chemical events, since they are easy to manufacture, scalable and versatile. In particular, semiconductor sensors for chemical and biological detection are more attractive, since label-free, point-of-care detection is possible with miniaturized sensor devices. Seyama showed that sensing gas is possible with simple electrical devices in 1960, and Naoyoshi Taguchi invented semiconductor gas sensors for inflammable gases in 1968.[1] Since 1980, much research and development have gone into semiconductor gas sensors, with progress in microfabrication technology and rapid growth in materials sciences. However, most of the semiconductor sensors in the market suffer from low selectivity and high power consumption, since they are generally based on metal oxide thin films or composites of metal oxide nanoparticles. (https://www.figaro.co.jp/en/technicalinfo/principle/mos-type.html).

Several key methods have been developed to increase the sensitivity and decrease the working temperature of semiconductor gas sensors, including the development of new sensor materials and engineering of semiconductor materials.

[a]*Advanced Materials Division, Korea Research Institute of Chemical Technology (KRICT), 141 Gajeong-ro, Daejeon 34114, Korea. E-mail: Jolee@krict.re.kr*
[b]*Department of Physics, Sungkyunkwan University, 2066 Seobu-ro, Suwon 16419, South Korea*
[c]*Center for Molecular Modeling and Simulation, Korea Research Institute of Chemical Technology (KRICT), Daejeon 34114, South Korea*
[d]*Department of Chemistry, Ulsan National Institute of Science and Technology (UNIST), Ulsan 689-798, South Korea*
[e]*Department of Materials Science and Engineering, University of Michigan, Ann Arbor, Michigan 48109, USA*
[f]*Department of Materials Science and Engineering, Korea Advanced Institute of Science and Technology, Daejeon, 34141, South Korea*
[g]*Department of BioNano Technology, Gachon University, Seongnam, Gyeonggi-Do 13120, South Korea*
[h]*Department of Mechanical Engineering, Korea Advanced Institute of Science and Technology (KAIST), Deajeon 34141, South Korea*
[i]*School of Mechanical Engineering, Sungkyunkwan University, Seobu-ro, Jangangu, Suwon, Kyunggi-do 16419, South Korea*
[j]*Department of Physics, Ulsan National Institute of Science and Technology (UNIST), Ulsan 689-798, South Korea*

† Electronic supplementary information (ESI) available: Statistical distribution, SEM, AFM, XPS, EFM, gas reactivity and sensitivities, optical image, electrical properties, long-term stability of sensor devices. See DOI: 10.1039/c9nr03984h

‡ Present address; Department of Nanostructured Materials, Leibniz Institute of Polymer Research Dresden, 01069 Dresden, Germany.

This journal is © The Royal Society of Chemistry 2019

View Article Online

Published on 29 July 2019. Downloaded by Korea Advanced Institute of Science & Technology / KAIST on 9/26/2019 4:29:01 AM.

In the case of new materials development, perovskite-based semiconductors are particularly promising candidates showing high sensitivity at RT,[2,3] even with stability issues present. From an engineering aspect, various methods including surface modification, additive doping and light activation[4–7] were developed for metal oxide gas sensors. Surface modification is particularly effective for microfabricated sensor materials, since the specific surface area greatly increases with decreasing size. Also, as reported by Tamvakos and colleagues, reducing the grain size of the material may directly lead to an increase in its sensitivity.[8] To fulfill the unmet needs in semiconductor sensors, sensors produced using nanotechnology were developed, and have shown some potential in sensitivity enhancement. Since the first development of carbon nanotube chemical sensors that work at room temperature (RT)[9] various top-down or bottom-up fabricated nanosensors were developed with the expectation that they would solve the problems of sensitivity and power consumption displayed by the previous sensors.[10–16] The number of publications in the field of nanotechnology-based semiconductor gas sensors has grown over the years, although this growth has slowed down since 2011.[17] However, no nanotechnology-based sensors (except for composite materials) have entered the market after almost 20 years of research and development, presumably due to the intrinsic problems of nanoscale materials, including their poor reliability and the high costs and poor reproducibility of their production. A uniform production of nanosensors is particularly difficult to achieve, and the lack of uniformity and resulting aberrantly high sensitivity levels of individual nanosensors actually can become a bottleneck for commercialization, since such sensitivity may directly lead to false signals. Instead of using a "single" nanomaterial, ensembles of nanomaterials can provide a compromise between sensitivity and reproducibility. For example, Cho *et al.* fabricated high-performance chemical sensors by using arrays of porous nanotubes (bottom-up),[18] and Gao *et al.* succeeded in increasing the sensitivity of sensors of hydrogen by using nanosphere lithography (top-down).[19] However, it remains difficult to precisely control the formation and placement of nanomaterials for fabricating devices, and only nanoparticle composites that sacrifice some sensitivity and working temperature are in use for commercial production.

Recently, Choi *et al.* have reported an aligned growth of single-wall carbon nanotubes (SWNTs) on scratched SiO_2 surfaces, and the alignment phenomenon was attributed to the different chemical composition inside the scratch.[20] Scratches result when two materials having different hardness values strike one another. By choosing the right pair of materials, it may be possible to define ultra-fine patterns and desired chemical compositions in the scratch. As cuts or scratches in the skin (wound) are more sensitive to external stimuli, it is possible that altered chemical functionality inside the scratch makes the semiconductor thin film more sensitive toward molecular binding, *i.e.*, sensitivity enhancement may occur with scratches. In the present study, we used scratch lithography to fabricate scratched thin film-based chemical sensors, and showed them to be highly sensitive chemical sensors at RT. Scratches were generated onto various metal oxide thin films, and topological and chemical characteristics of the scratches were explored. Scratched thin films were made into sensor devices using conventional microfabrication technology, and the sensitivity levels of these films toward gas molecules (NO_2, NH_3) were compared with that of a control film without any scratch. Finally, in order to determine the mechanism underlying the operation of such scratch sensors, computational simulations based on density functional theory were performed, to specifically characterize the interactions of the gas molecules with the scratch sites.

2. Experimental

2.1 Thin film growth

ZnO thin films were deposited on Si wafers (4 inch) with 300 nm thick thermal SiO_2 using the ALD system (LUCIDA-D100) at a growth temperature of 150 °C. The self-regulating ALD process window was observed near 150 °C, and the entire deposition process was performed at this temperature. All substrates were cleaned before the deposition with acetone, then ethanol and finally deionized water. Conventional diethyl zinc (DEZn) and H_2O, cooled to 5 and 10 °C, respectively, were used as reactants for the synthesis of ZnO. The exposure times of DEZn and H_2O were 0.5 s and 0.2 s, respectively. After every exposure step, 10 s of purging was performed to eliminate the residual materials on the substrate (DEZ injection–purge–H_2O–purge cycle). N_2 with a purity of 99.99% was used for the delivery of precursors and for the purging. The N_2 flow rate was set to 100 sccm through the mass flow controller. The thickness of every ZnO film sample was controlled only by changing the number of ZnO growth cycles, and information about the increase in the ZnO thickness was confirmed using spectroscopic ellipsometry (Horiba Jobin Yvon UVISEL).

2.2 Scratch lithography and device fabrication

Nanoribbon devices were produced by using "scratch lithography", specifically by using a polishing machine (Digiset-1 V Metkon). Before application of the scratch lithography, a water-based polycrystalline diamond suspension (Allied High Tech, 0-32015) was sprayed onto an 8 inch microcloth (Buehler) on a rotating polishing disk (diamond diameter = 1 μm). ZnO deposited on a SiO_2/Si chip (2 cm × 2 cm) was flipped upside-down and pressed on the microcloth during rotation of the polishing disk for 3 s. After the scratch lithography, the diamond suspension that remained on the sample surface was removed by ultrasonically cleaning the surface with de-ionized water (DI-W), and we name such fabricated samples as S-ZnO (scratched ZnO). Finally, ZnO or S-ZnO on the SiO_2/Si chip was covered with a 500 μm × 500 μm metal stencil mask and aluminum (Al) metal was deposited by carrying out thermal evaporation (Al electrode thickness: 60 nm).

View Article Online

Published on 29 July 2019. Downloaded by Korea Advanced Institute of Science & Technology / KAIST on 9/26/2019 4:29:01 AM.

Electrical characters of ZnO and S-ZnO were measured using a Keithly semiconductor parameter analyzer (S2400). In order to measure current–voltage (I–V) and transfer characteristics (I–V_g), bias voltage was applied to screen printed electrodes on top of the sample, using highly p doped silicon substrate itself as a backgate.

2.3 Characterization

Binding component analyses for the metal oxide materials were conducted by performing XPS (using a Thermo Scientific K-Alpha instrument) with the incident beam produced by an Al X-ray source ($h\nu$ = 1486.6 eV) and a pass energy of 50 eV. Also charge distribution analyses of material surfaces were performed using an electrostatic force microscopy (EFM) system (Bruker Multimode 8 controller) in a fixed lift mode (100 nm) with Co/Cr-coated MESP tips (Bruker, frequency, 75 kHz) and with controlled applied voltages (0–10 V). The gas sensor data were obtained using VTS Corporation gas sensor equipment. The sensor devices were placed into a sample holder in a vacuum chamber and evacuated with a rotary pump for several hours in order to stabilize the chamber. After evacuation, the gas sensor response test was performed by repetitively turning on and off the gas (each for 250 s) at room temperature. The gas concentration was controlled by adjusting the gas flow (sccm) in 1000 ppm NO_2 gas. After the gas sensing test, a UV response analysis was performed by using a portable UV radiation system (Vilber Lourmat, 6 watt, 365 nm wavelength). The humidity response test was performed using a Sourcemeter (Keithley 2636B). Total flow rate is fixed at 500 sccm and use the controlled N_2 balancing gas and H_2O bubbling gas.

2.4 Computer calculation details

To perform the first-principles calculations, we employed the Vienna *Ab initio* Simulation Package (VASP) source code,[21,22] and the atomic pseudopotentials used in this paper were designed by using the Projector Augmented Wave (PAW) method as provided with the aforementioned package.[23] A plane-wave basis set with an energy cutoff of 700 eV and the Perdew–Burke–Ernzerhof (PBE) type gradient-correlated functional were used to describe the exchange–correlation potential. We modeled the four-layer ZnO (0001) substrate and four-layer TiO_2 (110) substrate with the 3 × 3 × 1 sampled k-point grids by using the Monkhorst–Pack scheme.[24] All of the model structures were relaxed until the self-consistent forces reached 0.02 eV Å^{-1}.

3. Results and discussion

3.1 Scratch lithography of ZnO films

To make scratches on semiconducting films, metal oxide thin films were made with atomic layer deposition (ALD) or sol–gel technique/sputter deposition, and then briefly polished using a diamond suspension. Details of these procedures are described in the Experimental section. Fig. 1a shows a schematic of the sample fabrication and physical characteristics of the scratches. As shown in the atomic force microscopy (AFM) image of Fig. 1b, uniform nanoscratch lines formed along the polishing direction, with a density of approximately ∼16 nanoscratch lines per micrometer (ESI Fig. S1†). Note that these scratches had widths of a few nanometers but lengths greater than hundreds of microns, dimensions nearly unachievable using other fabrication methods. Drawings next to the AFM images are the expected molecular structures of ZnO subjected to scratching (S-ZnO) and pristine ZnO (details in the following Calculation section). The density of scratched lines can be controlled either by changing the size of the diamond particles and/or by changing the duration of scratching.[20]

Along with the physical characteristics of the scratch, chemical compositions of scratch lines were explored using X-ray photoemission spectroscopy as shown in Fig. 1c and d. In general, ZnO is characterized by two main peaks: for Zn 2p at ∼1022 eV, and for O 1s at ∼530 eV.[25–27] As shown in the figure, both the Zn 2p and O 1s peaks from our sample exhibited small red shifts. These deconvolutions of the peaks revealed the presence of more metallic Zn and defect oxygens with the scratch process, but fewer zinc hydroxide and hydroxyl groups. This result was consistent with that of the previous study by Choi *et al.*, which showed the presence of low-oxidation-state SiO_{2-x} in scratched SiO_2.[20]

To determine whether the change in the chemical composition resulting from the application of scratch lithography is specific to the scratching procedure, we compared the XPS spectrum of the S-ZnO thin film with that of ZnO nanorod ground with a mortar and pestle (ESI Fig. S2 and S3†). Although both procedures used mechanical forces, the chemical compositions of the resulting materials differed: while the ground ZnO nanorod also showed an increase in oxygen defects, the increase in the amount of metal characteristic of the scratch method was not observed. Perhaps this difference resulted from the use of different tribological pairs, *i.e.*, ZnO–diamond *versus* ZnO–ZnO. Recent work by Wang and colleagues showed that phase-transformed Si nanostructures were formed by scratching or grinding the surface with a diamond tip.[28] Given that a diamond tip may generate ∼5.11 GPa stress in silicon when inducing phase changes,[28] it is reasonable to expect that the stress created by ZnO would not be sufficient to induce a phase change. We also showed there to be a lack of dependence of the scratch-induced chemical composition change on the deposition method used to produce the film: similar changes of the XPS spectra upon scratching were observed for ZnO thin films produced using ALD and those produced using the sol–gel method (ESI Fig. S4 and S5†). And, strikingly, we also found such scratch-induced changes in chemical composition for other kinds of metal oxides, namely In_2O_3, SnO_2 and TiO_2 (ESI Fig. S6, S7 and S8†) as has Choi *et al.* for SiO_2.

3.2 Gas sensor measurements with scratched devices

As shown in the previous paragraphs, physical and chemical characteristics of the ZnO thin films were observed to change upon being scratched. In order to investigate the effects of

 This journal is © The Royal Society of Chemistry 2019

View Article Online

Published on 29 July 2019. Downloaded by Korea Advanced Institute of Science & Technology / KAIST on 9/26/2019 4:29:01 AM.

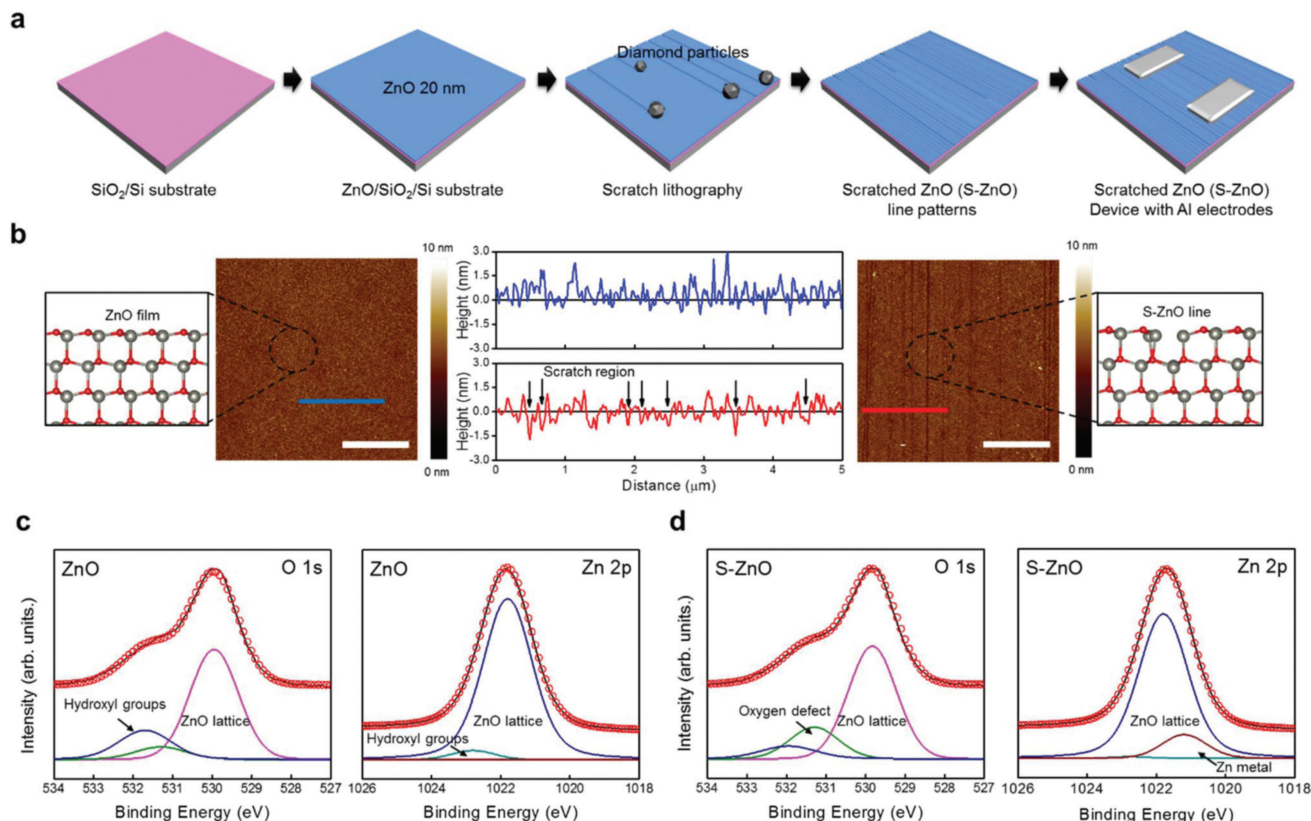

Fig. 1 Fabrication of ZnO scratch line patterns using scratch lithography. (a) Schematic diagram of the scratched ZnO (S-ZnO) fabrication process on Si/SiO_2. (b) AFM image of an ALD grown ZnO film (left) and that of S-ZnO. Cross sectional profiles of control ZnO (blue lines) and S-ZnO (red) are shown in the middle. Drawings in the box show the molecular diagram of ZnO and S-ZnO. Scale bar; 3 μm. (c) and (d) O 1s peak has been fitted using three peaks: ZnO lattice in pink (529.9 eV), oxygen defect in green (531.4 eV), and hydroxyl groups of ZnO in blue (531.7 eV). Zn 2p has also been fitted by using three peaks: zinc hydroxide in dark cyan (1022.8 eV), ZnO lattice in navy (1021.7 eV), and Zn metal in wine (1021.1 eV).

scratching on sensor performances, we compared the NO_2 and NH_3 gas-sensing characteristics of the control ZnO film device and the S-ZnO device, as shown in Fig. 2. The sensor data resistance values are shown converted to a $\log_{10}$ scale. All measurements were taken in a chamber with an N_2 atmosphere, and sensor responses were recorded at RT. The ZnO film device showed an ∼4% change in resistance when subjected to a 1000 sccm flow of 1000 ppm NO_2, and took more than 200 s to become saturated. For 1000 sccm of 1% NH_3, the ZnO film device showed no response at RT. In contrast, the S-ZnO device showed a ∼100% response to 1000 sccm of 1000 ppm NO_2, with a very rapid response (ZnO ∼0.8, S-ZnO ∼88015.4 $\Omega\ s^{-1}$ ($\Delta R/\Delta s$)). Dramatically enhanced sensitivity of S-ZnO is better described in ESI Fig. S9,† where the sensitivities are compared on the same scale. ESI Fig. S9 and S10† show the sensitivities and response times of control ZnO and S-ZnO sensors toward NO_2. Also, the ZnO film device that was unresponsive to NH_3 exposure showed a ∼7% response with the scratch process, although the response time was not as short as in the case of NO_2 exposure. Both the film device and scratched sensor device did not recover upon being refreshed with N_2, as shown in Fig. 2. A slow recovery could be a serious drawback for a sensor that requires continuous operation. A heater is commonly used with metal oxide sensors to increase their recovery rates. But since low-power heaters require thoughtful design and a complicated fabrication procedure, we considered the possibility of using UV light for refreshing the sensor device. In fact, ZnO itself is known to be a very good sensor of UV light. As shown in Fig. 2c and f, we compared the responses of the sensors to 365 nm wavelength UV light (6 watt). Surprisingly, while the ZnO film sensor showed a ∼60% response to UV light, the scratched device showed a ∼8000% response toward the same UV light. The response time of the scratched ZnO film device (23 s) was also shorter than that of the unscratched one (30 s). Therefore, as expected, scratched ZnO thin films showed greatly enhanced sensor performances for both chemical reaction and UV light exposure.

3.3 Mechanism of sensitivity enhancement

To determine why the introduction of scratches made the film so sensitive, we considered three possibilities: scratch-induced increase in surface area, changed topological feature, and altered chemical composition in the scratch.

First, to determine the effects of increased surface area, we fabricated ZnO thin-film sensor devices on filter paper. Fig. S11† shows photographs of the ZnO thin-film devices on

Published on 29 July 2019. Downloaded by Korea Advanced Institute of Science & Technology / KAIST on 9/26/2019 4:29:01 AM.

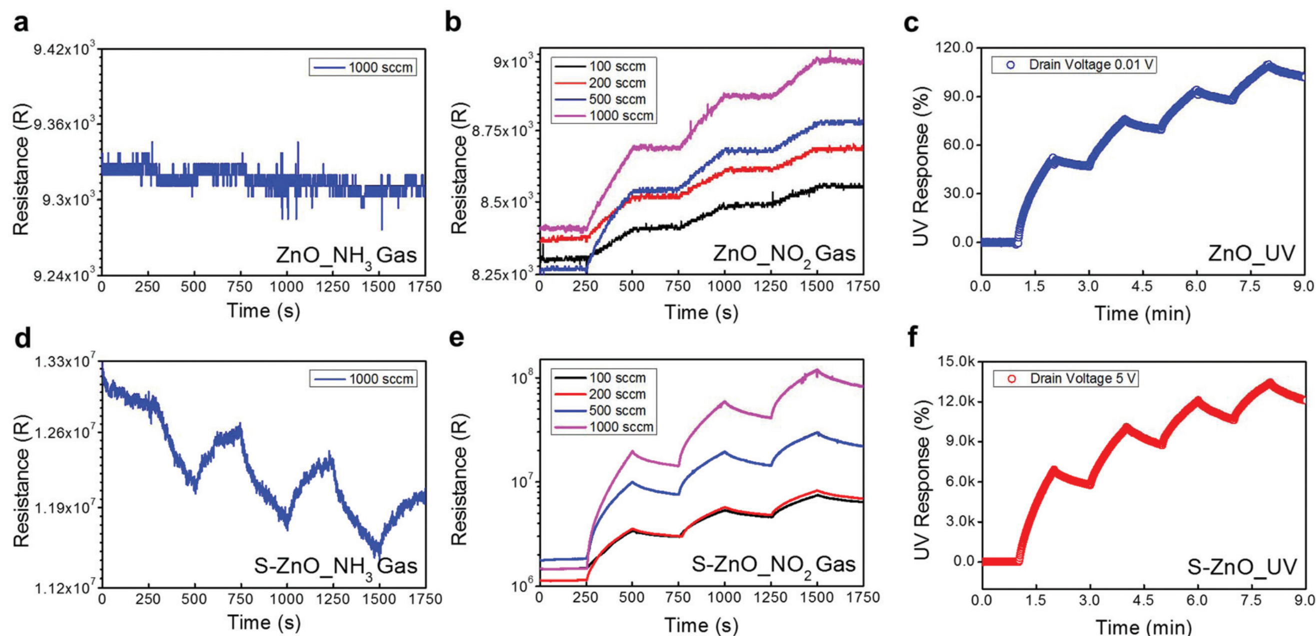

Fig. 2 Performances of ZnO and S-ZnO as sensors. Sensor data for the (a), (b), (c) ZnO film and (d), (e), (f) S-ZnO film. Target gases for the gas sensor test were (a), (d) NH_3 and (b), (e) NO_2 with the flow of the gases alternating between being on for 250 s and off for 250 s (here R denotes the resistance of devices). (c), (f) UV light (365 nm wavelength) response data at room temperature after sensor response measurement for the (c) ZnO and (f) S-ZnO films. Here UV response is defined as $(R_t - R_0)/R_0$.

porous filter paper, and the responses of these devices to NO_2 and UV illumination. As shown in the figure, the responses of these sensors were better than those of the devices on a smooth substrate, but worse than those of the scratched device. Fig. S11b† shows an EDS color map of the filter paper coated with ZnO. As shown in the figure, ZnO penetrated deep into the filter paper, effectively increasing the surface area. Therefore, the increased surface area may contribute to improved sensor performances, but cannot be the main reason. The surface area of the scratched film was estimated to be roughly three times that of the unscratched film (based on the ZnO thin film considered as a slab, and modeled so that the scratching transformed it into 15 thin slabs), not enough to support the dramatic increases in sensor responses (30-fold increase for NO_2 detection).

Second, a change in the topology of the film, specifically the formation of nanoribbons from films upon introduction of scratches, could be the main reason for the enhanced sensitivity of the scratched film. Fig. 3a and b show, respectively, transfer (I–V_g) characteristics and current–voltage (I–V) of a 20 nm thick ALD-grown ZnO thin film. The device showed a nearly metallic character, despite its relative thinness, presumably due to unintentional doping from the deposition process, and/or due to a small number of oxygen defects.[29,30] Beh and colleagues showed that ZnO thin films grown using ALD exhibited quasi-metallic behavior depending on the deposition temperature, and hydrogen-induced donor states were responsible for such behavior.[31] After introduction of the scratches, the device showed n-type semiconducting characteristics, while device resistance increased almost 10-fold, as shown in Fig. 3d and e. Since the polishing process we used to scratch the film likely "scrubbed off" the surface, an increase in the film resistance was inevitable, which requires higher bias voltages. More importantly, since the scratch lines were made with ~1 μm diameter diamond particles, deep scratch lines cut into the ZnO film so that arrays of ZnO nanoribbons formed on the entire surface. As shown in the ESI Fig. S12,† I–V measured perpendicular to the scratch direction yielded resistance values greater than a few hundred GOhms, helping to indicate that ZnO thin films were separated into nanoribbon arrays by the scratch process. Moreover, traces of scratches were present on the SiO_2 substrate after removing the S-ZnO with a dilute HNO_3 solution, as shown in Fig. S13.† Reduction of response time can also be explained by the nanosized topology of the nanoribbons on the scratched film. Since nanoribbons have three-dimensional faces analogous to the fin field-effect transistor (FinFET),[32] the exposed surface area and thus probability of gas molecule adsorption increased. Nevertheless, considering the thickness of the depletion layer (~10 nm)[33] of ZnO, which can be found in the field-effect transistor, gas molecules with a strong dipole moment are sufficient to tune the Fermi energy level of the nanosized 'fin' ZnO scratched device, making it very susceptible to its environment.

It is also interesting to note that the quasi-metallic ZnO thin film grown using ALD exhibited typical metal oxide semiconductor field-effect transistor (MOSFET) behavior after the scratching process; saturation of the drain current was appar-

This journal is © The Royal Society of Chemistry 2019

Published on 29 July 2019. Downloaded by Korea Advanced Institute of Science & Technology / KAIST on 9/26/2019 4:29:01 AM.

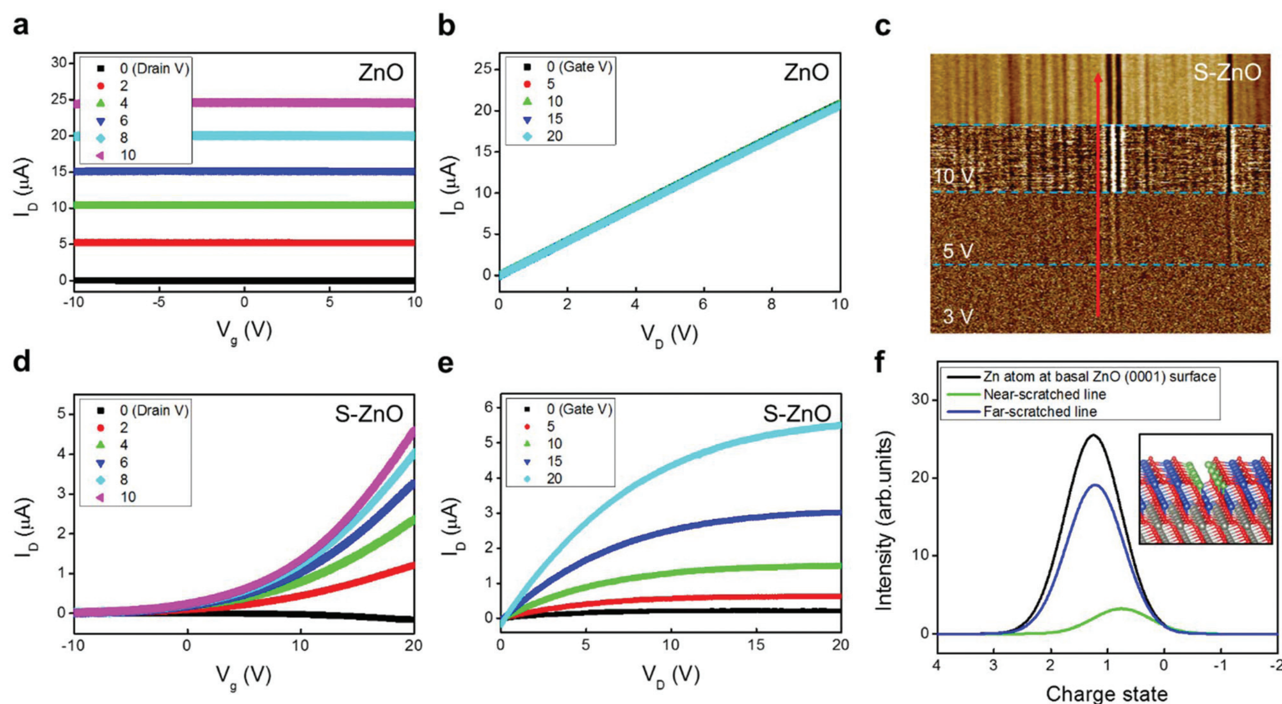

Fig. 3 Mechanism of the scratch effect. (a) and (b) Transfer and output characteristics of the ZnO device. The transfer characteristics were each measured with drain voltages of 0–10 V. (d) and (e) Transfer and output characteristics of the S-ZnO device. The transfer characteristics were each measured with drain voltages of 0–20 V. (c) EFM images of the S-ZnO surface at various applied voltages (0, 3, 5, 10 V) with a fixed tip lift height of 100 nm. (f) Charge states of Zn atoms situated at the basal ZnO (0001) surface (black line), at a scratch (green line), and at positions distant from a scratch (blue line). The green and blue balls in the inset indicate the positions of Zn atoms for the green and blue lines, respectively.

ent due to the pinch off effect. The observed saturation of the drain current is quite reasonable; the metallic thin film became semiconducting upon being subjected to scratch lithography, as shown in Fig. 3. It is also possible that sensitivity enhancement originated from metal–semiconductor transition, since the working principle of the metallic film (chemiresistor mode) would be different from that of the semiconducting film (FET mode). Yet, as shown in the ESI Fig. S14 and S15,† sensitivity enhancement is also prominent for S-ZnO devices fabricated with semiconducting ZnO. In that case, the gate threshold voltage of S-ZnO moves toward further positive gate voltages, applying gate bias voltage is necessary for sensor operation. Considering the advantage of two-terminal devices over three-terminal FET, S-ZnO devices fabricated with heavily doped ZnO as shown in the present study are more promising for practical applications. Many different ZnO nanostructure morphologies, including ribbons, wires, and rods, have been fabricated and reported to display enhanced semiconducting properties;[16,34–38] compared to previously reported methods, the scratching method has the significant advantage that it can be directly integrated into the thin film based fabrication process that is widely used in the current industry.

Finally, the effects of the altered chemical composition in the scratch were investigated using computational simulations based on density functional theory. Details regarding the computational simulation are provided in the Experimental section. As the above-described XPS results showed, Zn–Zn binding appeared and the amount of lattice oxygen decreased when we scratched the ZnO (0001) surface. From that result, we modeled the oxygen line defect on the ZnO (0001) surface. Schematics of the ZnO and S-ZnO models we used are shown in Fig. 1. We performed calculations using the model and checked that the Zn dimer formed as the result of geometry optimization calculation as in Fig. 1b. As shown in Fig. 3f, the S-ZnO model showed a different charge state along the scratch lines; while an electric force microscopy (EFM) analysis indicated a high accumulation of charges along the scratches, as shown in Fig. 3c. We computed the Bader charges of various types of Zn atoms, including those at the basal site, at a scratch, and distant from a scratch, and plotted the charges in Fig. 3f by using the Gaussian broadening method. With oxygen atoms scratched out, the chemical formula of the near-scratched site became ZnO_{1-x} (with $x > 0$) and the Zn atoms here had more electrons than did those at the basal site. Due to the lack of oxygen atoms, the Zn atoms at the scratch site became less positively charged. However, no difference was indicated between the charge state of the sites distant from the scratch and that of the basal site. Therefore, EFM analysis and charge state simulation showed only a localized influence of the scratch and an ability of the scratch to change the charge state of the Zn atoms.

After preparing the surface models, various gas species such as NH_3, NO_2, NO, CO, and H_2 were made to adsorb onto

Published on 29 July 2019. Downloaded by Korea Advanced Institute of Science & Technology / KAIST on 9/26/2019 4:29:01 AM.

Table 1 Binding energies (in units of eV) of various gases, including NH_3, NO_2, NO, CO, and H_2, for the ZnO, scratched ZnO (S-ZnO), TiO_2, and scratched TiO_2 (S-TiO_2) surfaces

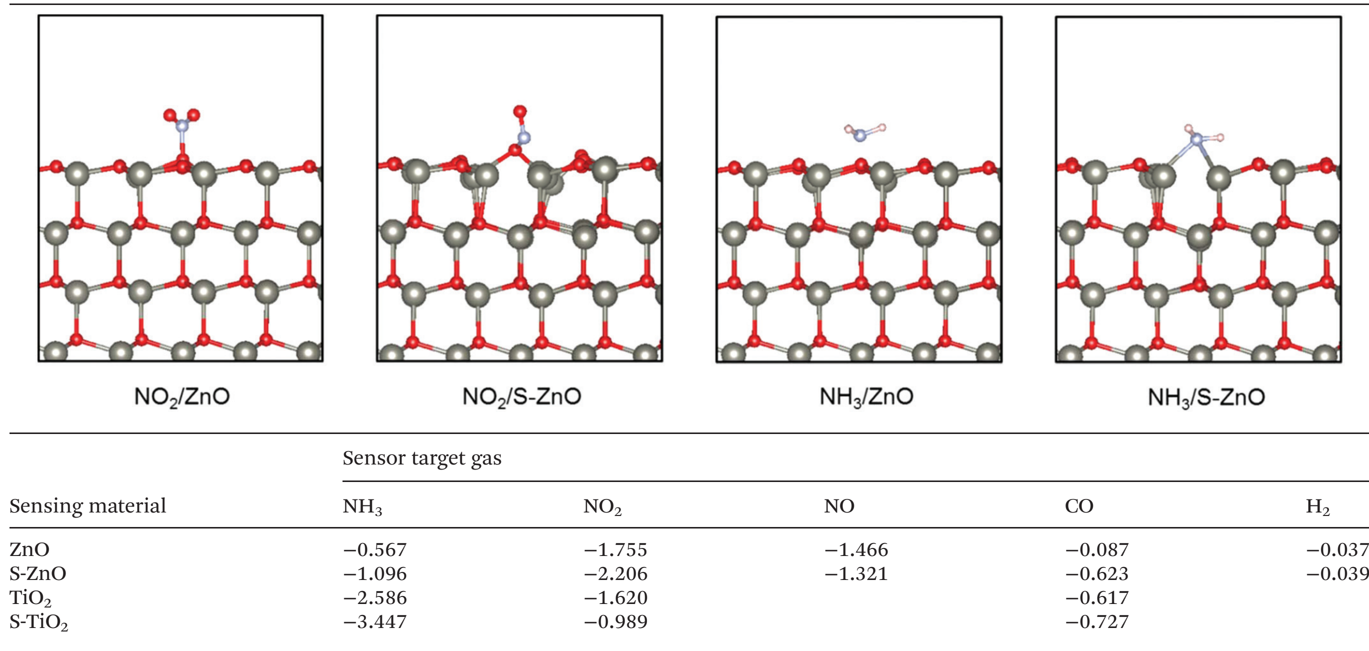

	Sensor target gas				
Sensing material	NH_3	NO_2	NO	CO	H_2
ZnO	−0.567	−1.755	−1.466	−0.087	−0.037
S-ZnO	−1.096	−2.206	−1.321	−0.623	−0.039
TiO_2	−2.586	−1.620		−0.617	
S-TiO_2	−3.447	−0.989		−0.727	

the prepared substrates, and the binding energy (E_B) values for those gases were calculated by using the equation

$$E_B = [E_{substrate} + E_{reference\ gas}] - E_{(gas-substrate)}$$

where $E_{substrate}$, $E_{reference\ gas}$, and $E_{(gas-substrate)}$ are the free energy values for the substrate, gas species, and gas-adsorbed system, respectively. Table 1 lists the calculated binding energies of gas molecules. In the case of ZnO, the calculated binding energies of the NH_3, NO_2, and CO gases dramatically increased when the surface was scratched, while the binding energies of the NO and H_2 gases showed negligible changes from ZnO. This trend of changes of binding energy was similar to the trend of the experimental results, which showed enhanced sensitivities of S-ZnO toward NH_3 and NO_2 gases.

To make sensor multiplexes and increase the range of target molecules, we also performed a similar calculation with TiO_2, as shown in Fig. S16.† As described above and in ESI† figures, the universality of the scratch technique was confirmed; that is subjecting In_2O_3, SnO_2 and TiO_2 (ESI Fig. S6, S7 and S8†) to this technique yielded increased amounts of the metal and defect oxygens. In the TiO_2 case, application of the scratch technique resulted in an increase in the binding energy of NH_3, a decrease in that of NO_2, and no change in that of CO. This result implied that by using different metal oxides or semiconductor materials, it is possible to make arrays of scratched sensor devices with unique gas selectivities.

Yet, metallic bonds formed with scratch lithography are susceptible to harsh environments. In ESI Fig. S17,† we obtained the XPS spectra of S-ZnO samples after annealing them at moderate temperatures of 100, 200, and 300 °C. As shown in the figures, while defect oxygen peaks produced with scratch lithography persist even after high temperature annealing, peaks corresponding to the metallic Zn component started to disappear at 200 °C. We believe the poisoning of scratch induced functional groups is responsible for the slight decrease in sensitivity after storing the S-ZnO sensors for two months (ESI Fig. S18†). Even with the loss of active functional groups, S-ZnO sensors showed much improved performances than their pristine counterparts, and were also stable up to 80% humidity (ESI Fig. S19†).

4. Conclusions

In summary, we explored the possibility of enhancing the sensitivity of sensor devices based on metal oxide thin films by using scratch lithography. Scratches made in the metal oxide thin films increased the surface area of the film, and effectively made the continuous thin film into arrays of nanoribbons, and also changed the chemical composition of the film so that certain chemical species bound more strongly onto the surface. The technique was also shown to be applicable to a variety of metal oxides and semiconductor thin films, and it hence may be possible to fabricate arrays of scratched sensor devices that selectively sense specific gas molecules. Finally, the scratch technique could, due to its scalability, versatility and ease of use, be generalized to fabricate nanoribbon devices on the industrial scale.

Conflicts of interest

Authors declare no conflict of interest.

This journal is © The Royal Society of Chemistry 2019

Published on 29 July 2019. Downloaded by Korea Advanced Institute of Science & Technology / KAIST on 9/26/2019 4:29:01 AM.

Acknowledgements

This research was supported by the Multi-Ministry Collaborative R&D Program (Development of Techniques for Identification and Analysis of Gas Molecules to Protect Against Toxic Substances) through the National Research Foundation of Korea (NRF) funded by KNPA, MSIT, MOTIE, ME, and NFA (NRF-2017M3D9A1073858), and by the Focused Research Program of the Korea Research Institute of Chemical Technology (KRICT).

References

1 G. Neri, *Chemosensors*, 2015, **3**, 1–20.
2 H. Chen, R. Bo, A. Shrestha, B. Xin, N. Nasiri, J. Zhou, I. Di Bernardo, A. Dodd, M. Saunders, J. Lipton-Duffin, T. White, T. Tsuzuki and A. Tricoli, *Adv. Opt. Mater.*, 2018, **6**, 1800677.
3 H. Chen, M. Zhang, R. Bo, C. Barugkin, J. Zheng, Q. Ma, S. Huang, A. W. Y. Ho-Baillie, K. R. Catchpole and A. Tricoli, *Small*, 2018, **14**, 1702571.
4 C.-L. Hsu, L.-F. Chang and T.-J. Hsueh, *Sens. Actuators, B*, 2017, **249**, 265–277.
5 L. Zhu and W. Zeng, *Sens. Actuators, A*, 2017, **267**, 242–261.
6 S. Mishra, C. Ghanshyam, N. Ram, R. P. Bajpai and R. K. Bedi, *Sens. Actuators, B*, 2004, **97**, 387–390.
7 C. B. Jacobs, A. B. Maksov, E. S. Muckley, L. Collins, M. Mahjouri-Samani, A. Ievlev, C. M. Rouleau, J. W. Moon, D. E. Graham, B. G. Sumpter and I. N. Ivanov, *Sci. Rep.*, 2017, **7**, 6053.
8 A. Tamvakos, D. Calestani, D. Tamvakos, R. Mosca, D. Pullini and A. Pruna, *Microchim. Acta*, 2015, **182**, 1991–1999.
9 J. Kong, *Science*, 2000, **287**, 622–625.
10 Z. Wang, X. Zhan, Y. Wang, S. Muhammad, Y. Huang and J. He, *Nanoscale*, 2012, **4**, 2678–2684.
11 T.-Y. Wei, P.-H. Yeh, S.-Y. Lu and Z. L. Wang, *J. Am. Chem. Soc.*, 2009, **131**, 17690–17695.
12 J. T. Robinson, F. K. Perkins, E. S. Snow, Z. Wei and P. E. Sheehan, *Nano Lett.*, 2008, **8**, 3137–3140.
13 A. Tricoli, M. Righettoni and A. Teleki, *Angew. Chem., Int. Ed.*, 2010, **49**, 7632–7659.
14 D. R. Miller, S. A. Akbar and P. A. Morris, *Sens. Actuators, B*, 2014, **204**, 250–272.
15 J. Liu, T. M. Fu, Z. Cheng, G. Hong, T. Zhou, L. Jin, M. Duvvuri, Z. Jiang, P. Kruskal, C. Xie, Z. Suo, Y. Fang and C. M. Lieber, *Nat. Nanotechnol.*, 2015, **10**, 629–636.
16 M. E. Franke, T. J. Koplin and U. Simon, *Small*, 2006, **2**, 36–50.
17 J. Mizsei, *Procedia Eng.*, 2016, **168**, 221–226.
18 I. Cho, K. Kang, D. Yang, J. Yun and I. Park, *ACS Appl. Mater. Interfaces*, 2017, **9**, 27111–27119.
19 M. Gao, M. Cho, H. J. Han, Y. S. Jung and I. Park, *Small*, 2018, **14**, 1703691.
20 W. J. Choi, Y. J. Chung, Y. H. Kim, J. Han, Y. K. Lee, K. J. Kong, H. Chang, Y. K. Lee, B. G. Kim and J. O. Lee, *Sci. Rep.*, 2014, **4**, 5289.
21 G. Kresse and J. Furthmüller, *Comput. Mater. Sci.*, 1996, **6**, 15–50.
22 G. Kresse and J. Furthmüller, *Phys. Rev. B: Condens. Matter Mater. Phys.*, 1996, **54**, 11169–11186.
23 P. E. Blochl, *Phys. Rev. B: Condens. Matter Mater. Phys.*, 1994, **50**, 17953–17979.
24 J. P. Perdew, K. Burke and M. Ernzerhof, *Phys. Rev. Lett.*, 1996, **77**, 3865–3868.
25 S. Jeong, Y. G. Ha, J. Moon, A. Facchetti and T. J. Marks, *Adv. Mater.*, 2010, **22**, 1346–1350.
26 S. Ben Amor, M. Jacquet, P. Fioux and M. Nardin, *Appl. Surf. Sci.*, 2009, **255**, 5052–5061.
27 J. Nakamura, I. Nakamura, T. Uchijima, Y. Kanai, T. Watanabe, M. Saito and T. Fujitani, *J. Catal.*, 1996, **160**, 65–75.
28 B. Wang, Z. Zhang, K. Chang, J. Cui, A. Rosenkranz, J. Yu, C. Te Lin, G. Chen, K. Zang, J. Luo, N. Jiang and D. Guo, *Nano Lett.*, 2018, **18**, 4611–4617.
29 Y. Jang Chung, W. Jin Choi, S. Gu Kang, C. Wan Lee, J.-O. Lee, K.-J. Kong and Y. Kuk Lee, *J. Mater. Chem. C*, 2014, **43**, 9274–9282.
30 J. Laube, D. Nübling, H. Beh, S. Gutsch, D. Hiller and M. Zacharias, *Thin Solid Films*, 2016, **603**, 377–381.
31 H. Beh, D. Hiller, M. Bruns, A. Welle, H.-W. Becker, B. Berghoff, C. Sürgers, R. Merz and M. Zacharias, *J. Appl. Phys.*, 2017, **122**, 025306.
32 X. Huang, W.-C. Lee, C. Kuo, D. Hisamoto, L. Chang, J. Kedzierski, E. Anderson, H. Takeuchi, Y.-K. Choi, K. Asano, V. Subramanian, T.-J. King, J. Bokor and C. Hu, *IEEE Trans. Electron Devices*, 2001, **48**, 880–886.
33 I. E. Paulauskas, G. E. Jellison, L. A. Boatner and G. M. Brown, *Int. J. Electrochem.*, 2011, **2011**, 1–10.
34 Z. Jing and J. Zhan, *Adv. Mater.*, 2008, **20**, 4547–4551.
35 J. Eriksson, V. Khranovskyy, F. Söderlind, P.-O. Käll, R. Yakimova and A. Lloyd Spetz, *Sens. Actuators, B*, 2009, **137**, 94–102.
36 A. Rothschild and Y. Komem, *J. Appl. Phys.*, 2004, **95**, 6374–6380.
37 C. Wang and W. Zeng, *J. Mater. Sci.: Mater. Electron.*, 2017, **28**, 10847–10852.
38 J. Nah, S. B. Kumar, H. Fang, Y.-Z. Chen, E. Plis, Y.-L. Chueh, S. Krishna, J. Guo and A. Javey, *J. Phys. Chem. C*, 2012, **116**, 9750–9754.